This version of the ESI published 03/10/2024 replaces the previous version published 23/09/2024.

In the text below the caption for Figure S4 "anhydride ring on the poly (isobutylene-maleic anhydride) " has been corrected to "lactam ring on the poly (succinimide)".

Supporting Information

Visualization of Drug Release in a Chemo-Immunotherapy Nanoplatform via Ratiometric ^{19}F Magnetic Resonance Imaging

Fanqi Liu, Xindi Li, Yumin Li, Suying Xu, Chang Guo* and Leyu Wang*

State Key Laboratory of Chemical Resource Engineering, College of Chemistry, Beijing University of Chemical Technology, Beijing 100029, China.

E-mail: lywang@mail.buct.edu.cn; guoc@mail.buct.edu.cn

Table of Contents

Experimental Procedures

Reagents and Chemicals.

Oleylamine (OAm) was supplied by Acros Organics. Adriamycin (Dox·HCl), Hydrogen peroxide, and 2-Mercaptoimidazole were bought from Aladdin. N, N-dimethylformamide (DMF), methanol (MeOH), ethanol (EtOH), dichloromethane (CH_2Cl_2), and *n*-hexane were all purchased from Tianjin Fuyu Fine Chemical Co., Ltd. Poly(succinimide) (PSI, MW ~ 2000 Da) were bought from Shijiazhuang Desai Chemical Company (China). Ammonium hydroxide ($NH_3·H_2O$), Zinc nitrate hexahydrate ($Zn(NO_3)_2·6H_2O$) and Histamine dihydrochloride (His) were obtained from Innochem. Sodium hydroxide (NaOH) was supplied by Tianjin Fuchen Chemical Reagent Co., Ltd. Nile Red was purchased from ShanghaiyuanyeBio-TechnologyCo., Ltd. Perfluoro-15-crown-5-ether (PFCE) was provided by Fluorochem Ltd. Pluronic F-127 (F127) was purchased from Sigma-Aldrich. Methyl thiazolyl tetrazolium (MTT) was supplied by Amresco Inc. Fetal calf serum (FBS) was provided by Hangzhou Sijiqing Bio-engineer Materials Ltd. Dulbecco's modified eagle medium (DMEM), phosphate-buffered saline (PBS) and trypsin were all bought from M&C Gene Technology Ltd. Caspase-1 Activity Assay Kit was obtained from Beyotime Biotech. Inc. Calcein/PI cell viability assay kit, 2′,7′-dichlorodihydro-fluorescein diacetate (DCFH-DA), mitochondrial membrane potential assay kit with JC-1, and ATP content were all purchased from Beyotime Biotech. Inc. DAPI and Anti-GSDMD polyclonal antibody were purchased from Solarbio. The anti-Calreticulin rabbit pAb, anti-HMGB1 rabbit pAb and FITC labeled goat anti-rabbit IgG were purchased from Servisebio. ATP assay kit was purchased from Beyotime Biotech. Inc. The brilliant Violet 421 anti-mouse CD86 and the APC anti-mouse CD80 were purchased from Bio Legend, Inc. Ultrapure water was used for all experiments. The mouse IFN-γ ELISA kit, mouse TNF-α ELISA kit, and mouse IL-6 ELISA kit were bought from Multi-Science. The FITC anti-mouse CD3 and APC anti-mouse CD8 were purchased from Beijing 4A Biotech Co., Ltd.

Instrumentation.

TEM images were acquired by using a JEOL JEM-1200EX (100 kV). Dynamic light scattering (DLS) particle size analysis was carried out with a Zetasizer Nano-ZS90 zeta and size analyzer from Malvern. UV-*vis*-NIR absorption spectra were recorded on a UV-3600 spectrophotometer (Shimadzu). ^{19}F nuclear magnetic resonance (NMR) experiments were carried out on a Bruker Avance-III HD 400 spectrometer at 376.47 MHz using a Bruker "single-pulse" sequence without proton decoupling. Fluorescence spectra were acquired by F-4600 fluorescence spectrophotometer (Hitachi). The cell viability was tested with a Tecan Infinite F50 (Switzerland) plate reader. Cellular fluorescence imaging was captured using a model eclipse Ti2−U inverted fluorescence microscope (Nikon). Tumor globular cell imaging was obtained using a Leica SP8 confocal laser scanning microscope (CLSM). The *in vitro* and *in vivo* MR imaging (^1H and ^{19}F) were acquired on a 7.0 T Bruker BioSpec70/20USR MRI system, using a transmitter and transceiver integrated $^1H/^{19}F$ birdcage coil for mouse body to detect ^1H and ^{19}F signals. Flow cytometry studies were performed with a Flow Cytometre Beamcyte-1026(BEAM DIAG) and a Flow Cytometre BD LSRFortessa (BD Biosciences). X-ray photoelectron Spectroscopy (XPS) experiments were obtained using an X-ray photoelectron Spectroscopy instrument ESCALAB 250 (THERMO VG). An inductively coupled plasma optical emission spectrometer (ICP-OES, Perkin Elmer, Avio 200) was adopted for the tests of Zn^{2+} content in the nanoplatforms.

Synthesis of 2-((2,2,2-trifluoroethyl)sulfinyl)-1*H*-imidazole.

2-Mercaptoimidazole (1.0 g), sodium bicarbonate (1.0 g), and 1,1,1-Trifluoro-2-iodoethane (4.0 mL) were mixed in methanol (15 mL) and stirred under reflux condensation at 65 °C for 24 h. Then, the mixed solution was dried by rotary evaporation. Thereafter, the product was extracted and collected by dichloromethane. The product 140 mg was dissolved into 800 μL acetone with 600 μL 10 M hydrogen peroxide at 37 °C and diluted with water for later use.

Preparation of amphiphilic polymer.

PSI (0.8 g) and His (0.0 g, 0.2 g, and 0.4 g, respectively) were mixed in DMF (12 mL) and stirred at 100 °C for 1 h. Then, OAm (0.8 mL) was added under magnetic stirring. After stirring at 100 °C for 24 h, the final product was precipitated with methanol and collected by centrifugation (8000 rpm, 6 min). The resulting final product with 0%, 15 and 30% grafting ratio of His was dissolved in DMF for further use, respectively.

Preparation of PF NPs and PF-Dox NPs.

For the preparation of PF NPs, the synthesized polymer ($PSI_{OAm/His}$, 5 mg) and PFCE (10 μL) were dissolved into a mixed solvent containing 0.7 mL of dichloromethane and 0.8 mL of DMF. The mixture was then added to 10 mL NaOH aqueous solution (0.6 mg, 1.2 mg, 1.6 mg, 2.0 mg), followed by ultrasonication treatment at 400 W for 6 min (3 s "on" and 3 s "off" in turn). The final product PF NPs was collected by centrifugation and redispersed in water for later use. In the synthesis of PF_3ZF NPs, a dosage of 1.6 mg of NaOH was used, while for the synthesis of $PF_{30}ZF$ NPs, a dosage of 0.6 mg of NaOH was employed.

For the fabrication of PF-Dox NPs, the synthesized polymer ($PSI_{OAm/His}$, 5 mg), PFCE (10 μL), and Dox (2 mg) were dissolved into a mixed solvent containing 0.7 mL of dichloromethane and 0.8 mL of DMF. The mixture was then added to NaOH aqueous solution (4 mM, 10 mL), followed by ultrasonication treatment at 400 W for 6 min (3 s "on" and 3 s "off" in turn). The final product PF-Dox NPs was collected by centrifugation and redispersed in water for later use.

For the synthesis of PF NPs-Nile red, the synthesized polymer ($PSI_{OAm/His}$, 5 mg), PFCE (10 μL) and Nile red (0.1 mg) were

dissolved into mixed solvent containing 0.7 mL of dichloromethane and 0.8 mL of DMF. The mixture was then added into NaOH aqueous solution (1.6 mg NaOH, 10 mL H_2O), followed by ultrasonication treatment at 400 W for 6 min (3 s "on" and 3 s "off" in turn). The final product PF NPs-Nile red for cell internalization experiment was collected by centrifugation and redispersed in water.

Preparation of PFZF NPs and PFZF-Dox NPs.

The as-prepared PF NPs or PF-Dox NPs (50 μg), $Zn(NO_3)_2 \cdot 6H_2O$ (1.95 mg), F127(0.7 mg) and 2-((2,2,2-trifluoroethyl)sulfinyl)-1*H*-imidazole (2.8 mg) were dissolved into H_2O (0.5 mL). Then $NH_3 \cdot H_2O$ (0.25 mL, 0.25%) was added under magnetic stirring. After stirring at room temperature for 15 min, the final product was collected and purified by centrifugation (18000 rpm, 15 min).

Zn^{2+} release under different conditions.

PFZF NPs colloidal solutions were incubated under different conditions (with different pH or incubation times). After centrifugation (18000 rpm, 20 min), the supernatant was digested thoroughly using aqua regia (V_{HCl} / V_{HNO3}= 3/1). The solutions were placed on a heating plate to volatilize the acid components and then made up to 8 mL using deionized water. The Zn^{2+} content of the samples was quantified using ICP-OES. Additionally, the Zn^{2+} content in the samples was quantified using ICP-OES, revealing a concentration of 7.16%.

Dox release under different conditions.

A standard curve was established by detecting the absorbance of PF-Dox NPs at different concentrations. PFZF-Dox NPs (0.4 mg/mL, 0.8 mg/mL, 1.6 mg/mL, or 2.4 mg/mL) colloidal solutions were incubated at different pH levels. After centrifugation (10000 rpm, 8 min), the supernatant was collected, and the absorbance was tested using a spectrophotometer. Additionally, the loading capacity of Dox was 0.85%, as determined by UV-vis spectroscopy.

***In vitro* ^{19}F NMR.**

^{19}F NMR spectra were all tested by utilizing a "single-pulse" sequence (a Bruker "zg" sequence). A capillary filled with D_2O was used to lock the field. The main parameters are as follows: spectral width (75000 Hz), accumulation number (128), FID size (65536), and acquisition time (0.437 s). The PFZF NPs colloidal solutions were tested under different pH.

Additionally, the integral area of ^{19}F NMR peak is proportional to the concentration of fluorine atoms within a certain linear range (Integral area = 5.615×10^6 C_F + 1.182×10^7, R^2 = 0.995). The PFCE and 2-((2,2,2-trifluoroethyl) sulfinyl)-1H-imidazole contents were assessed *via* ^{19}F NMR spectroscopy, yielding values of 3.64% and 15.82%, respectively.

Cell uptake and permeation

4T1 cells line was obtained from the Hunan Fenghui Biotechnology Co., Ltd (Changsha, China). 4T1 cells were seeded into a 12-well plate for 24 hours; after that, they were incubated with PFZF NPs for 0 h, 0.5 h, 1 h, 2 h, 4 h, 6 h, 8 h, or 10 h, respectively. Cells were stained with DAPI for 20 min. After washing with PBS, Cells were tested using a fluorescence microscope at 488 nm and 610 nm. The 3D multicellular tumor cell spheroids (MCTS) were incubated with PF_3ZF NPs and $PF_{30}ZF$ NPs for 2.5 h. Then, the MCTS were tested using a CLSM.

***In vivo* ^{19}F NMR.**

The *in vivo* ^{19}F NMR were taken on a 7.0 T Bruker BioSpec MRI system. ^{19}F NMR spectra in Figure 4E were all tested by utilizing a "single-pulse" sequence (a Bruker "NSPECT" sequence). The main parameters are as follows: spectral width (100000 Hz), accumulation number (50), FID size (4096), and acquisition time (50 s).

***In vivo* ^{1}H and ^{19F} MRI.**

The MR images were taken on a 7.0 T Bruker BioSpec MRI system. The T2-RARE (rapid acquisition with refocused echoes) method was employed for ^{1}H MRI. The repetition time (TR) and the echo time (TE) were 3000.00 ms and 40.00 ms, respectively. The matrix size was 256 × 256. The T1-RARE method was applied for ^{19}F MRI, and the parameters were fixed as follows: the number of accumulations was 20; TR and TE were 3000.00 ms and 22.52 ms, respectively. The field of view was 50 mm × 50 mm, and the matrix size was 100 × 100 with 19 min of accumulation time.

Cytotoxicity test.

4T1 cells were seeded in a 96-well cell culture plate at a density of 1×10^4 per well and incubated at 37 °C in 5% CO_2 for 24 h. The cells were treated with different concentrations of PFZF NPs, PF-Dox NPs free Dox, and PFZF-Dox NPs, respectively. After 24 h, cell cytotoxicity was detected by MTT assay.

ROS generation assay.

4T1 cells were seeded in a 6-well plate. Then they were treated with (I) PBS, (II) PFZF NPs (50 μg/mL), (III) PF-Dox NPs, (IV) Free Dox, (V) PFZF-Dox NPs at the same Dox concentration (0.42 μg/mL) for 6 h. After that, the cells were washed with PBS and stained with DCFH-DA for 30 min. The cells were tested using a fluorescence microscope at 525 nm.

Measurement of Mitochondrial Membrane Potential.

4T1 cells were seeded in a 12-well plate treated with various formulations: (I) PBS, (II) PFZF NPs (50 μg/mL), (III) Free Dox, (IV) PF-Dox NPs, (V) PFZF-Dox NPs, at the same Dox concentration (0.42 μg/mL) for 6 h. After washing with PBS, the cells were stained with 10 μm JC-1 for 30 min. The labeled cells were observed under a fluorescence microscope.

Wound Healing Assay

Cells were cultured in a 12-well plate until cells were confluent or nearly (>90%) confluent. Cell monolayers were scratched using a 200 μL pipette tip and then washed with PBS. After that, the cells were incubated with (I) PBS, (II) PFZF NPs (25 μg/mL), (III) Free Dox, (IV) PF-Dox NPs, (V) PFZF-Dox NPs, at the same Dox concentration (0.21 μg/mL) for 16 h. Finally, the cells were stained with DAPI for 20 min. Cell migration in the wound area was observed using a fluorescence microscope.

Western blot.

For western blots of GSDMD expressions, 4T1 cells were seeded into a 6-well plate treated with (I) PBS, (II) PFZF NPs (50 μg/mL), (III) Free Dox, (IV) PF-Dox NPs, (V) PFZF-Dox NPs, at the same Dox concentration (0.42 μg/mL) for 12 h. The cells were washed repeatedly with PBS and collected for a standard western blot process. For western blots of Caspase-1 expressions, 4T1 cells were seeded into a 6-well plate treated with (I) PBS, (II) PFZF NPs (50 μg/mL), (III) Free Dox, (IV) PF-Dox NPs, (V) PFZF-Dox NPs, at the same Dox concentration (0.42 μg/mL) for 12 h. The cells were washed repeatedly with PBS and collected for a standard western blot process.

***In Vitro* Assays of Immunogenic Cell Death.**

4T1 cells were seeded into a 6-well plate for 24 hours. Then, the cells were incubated with (I) PBS, (II) PFZF NPs (50 μg/mL), (III) Free Dox, (IV) PF-Dox NPs, (V) PFZF-Dox NPs, at the same Dox concentration of 0.42 μg/mL for 12 h. The culture medium from each well was collected and detected using an ATP detection kit.
4T1 cells were seeded into a 6-well plate for 24 hours, followed by incubation with (I) PBS, (II) PFZF NPs (50 μg/mL), (III) Free Dox, (IV) PF-Dox NPs, (V) PFZF-Dox NPs, at the same Dox concentration of 0.42 μg/mL for 12 h. The cells in each group were centrifuged, washed, and incubated with anti-CRT primary antibody for 2 h at 37 °C. Then, the cells were washed with PBS and incubated with FITC-labeled secondary antibody for 1 h. Finally, the cells were stained with DAPI for 20 min. The expression of CRT on 4T1 cells was measured using a fluorescence microscope.
4T1 cells were seeded into a 6-well plate for 24 hours, followed by incubation with (I) PBS, (II) PFZF NPs (50 μg/mL), (III) Free Dox, (IV) PF-Dox NPs, (V) PFZF-Dox NPs, at the same Dox concentration (0.42 μg/mL) for 12 h. The cells in each group were centrifuged, washed, and incubated with anti-HMGB1 primary antibody for 2 h at 37 °C. Then, the cells were washed with PBS and incubated with FITC-labeled secondary antibody for 1 h. Finally, the cells were stained with DAPI for 20 min. The expression of HMGB1 on 4T1 cells was measured using a fluorescence microscope.

***In Vitro* ICD-Induced Maturation of Dendritic Cells.**

DC 2.4 cells line was obtained from the Hunan Fenghui Biotechnology Co., Ltd (Changsha, China). In order to study the maturation of DC induced by ICD, a 24-well transwell system with 0.4 μm polycarbonate porous membrane was used. 4T1 cells were seeded in the upper wells at a density of 1×10^5 cells per well with 1 mL of medium and incubated 12 h, followed by incubation with (I) PBS, (II) PFZF NPs (50 μg/mL), (III) Free Dox, (IV) PF-Dox NPs, (V) PFZF-Dox NPs, at the same Dox concentration of 0.42 μg/mL for 12 h. Meanwhile, DC 2.4 cells were seeded in the lower wells at a density of 2×10^5 cells per well with 1 mL of medium and incubated for 24h. Then, the 4T1 cells in the upper wells and DC 2.4 cells in the lower wells were co-cultured in the medium 12 h. After that, the cells in the bottom wells were collected and stained with APC anti-mouse CD80/Brilliant Violet 421 anti-mouse CD86 for 15 min, which was further washed with PBS and resuspended at a density of 1×10^6 cells in 100 μL of PBS for flow cytometry assays.

Animals and tumor model.

All experiments involving animals were performed in accordance with the guidelines of the Institutional Animal Care and Use Committee (IACUC) of the China−Japan Friendship Hospital and Beijing University of Chemical Technology. The 4T1 subcutaneous tumor model was accomplished by injecting 4T1 cells into subcutaneous tissue. Five-week-old BALB/c mice (Female) with an average weight of 15 g were provided by SPF Biotechnology Co., Ltd. 5×10^6 per 4T1 cells were perfusion into a mouse subcutaneous tissue for establishing a proximal tumor model. After 12 days, 5×10^6 per 4T1 cells were perfusion into a mouse subcutaneous tissue for establishing a distal tumor model. Proximal mouse tumors in mice were injected with (I) PBS, (II) PFZF NPs,

(III) PF-Dox NPs, and (V) PFZF-Dox NPs. Mouse serum from different treatment groups was collected for ELISA detection. Mouse tumors were collected for section staining and flow cytometry detection.

Supplemental Figures

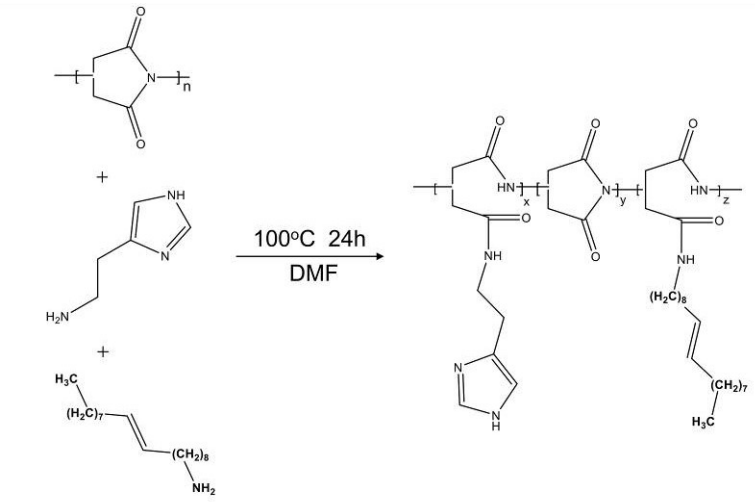

Figure S1. Synthetic routes of amphiphilic polymers.

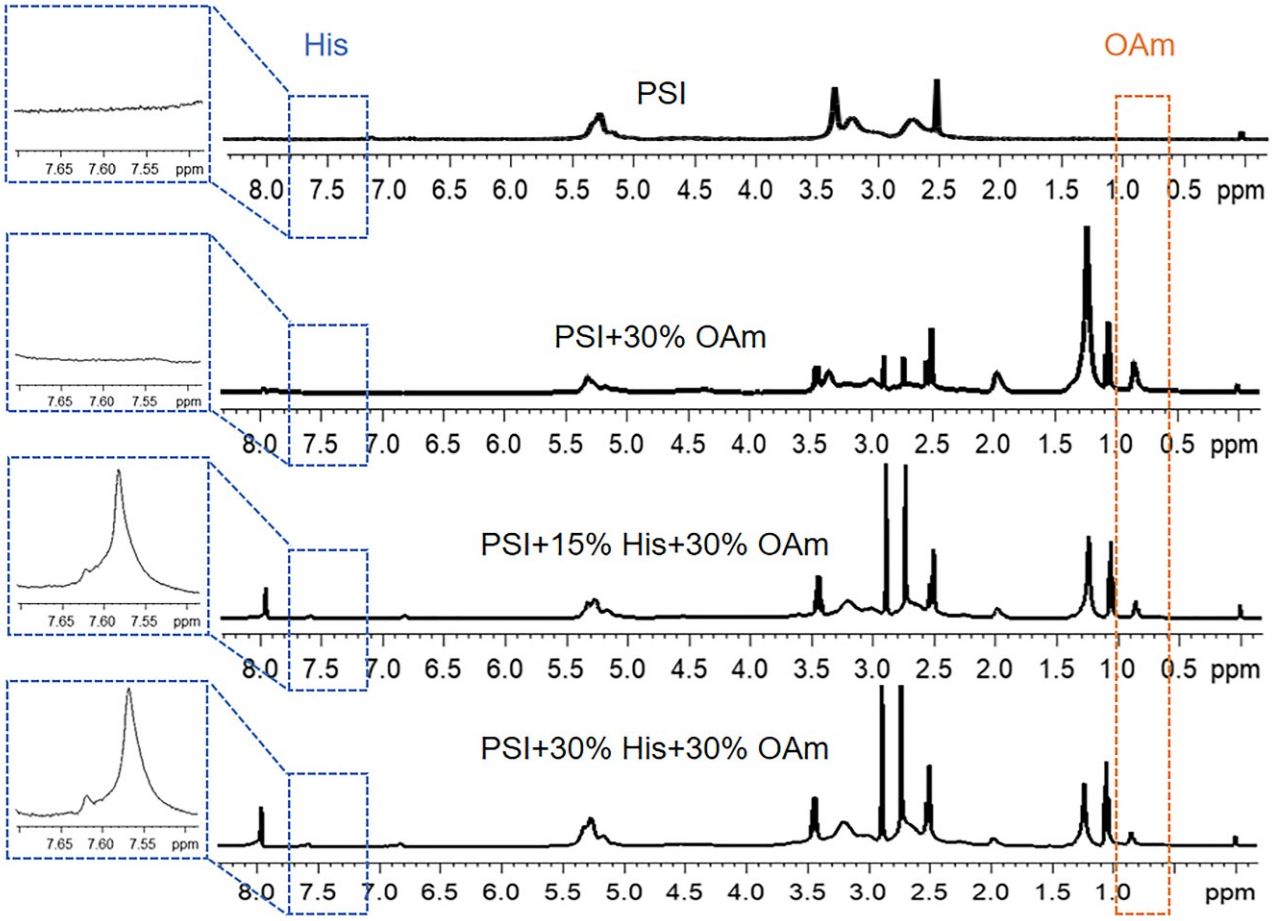

Figure S2. ^{1}H NMR spectra of amphiphilic polymers ($PSI_{OAM/His}$) with different grafting ratios of Histamine (His).

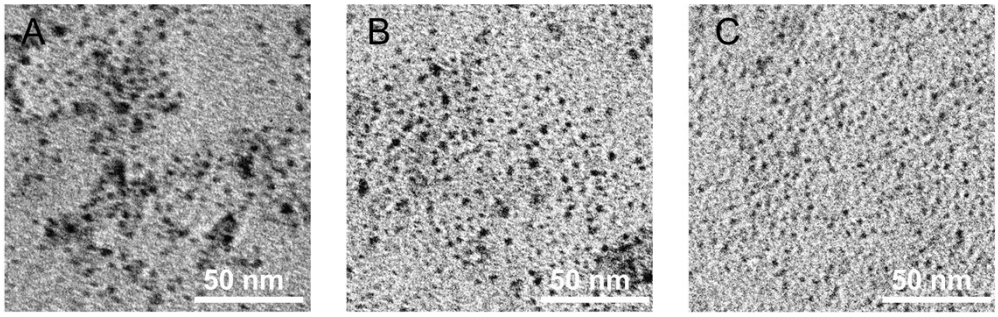

Figure S3. TEM images of PF NPs synthesized using polymers prepared with different grafting ratios of His, (A) 0%, (B) 15%, and (C) 30%, respectively.

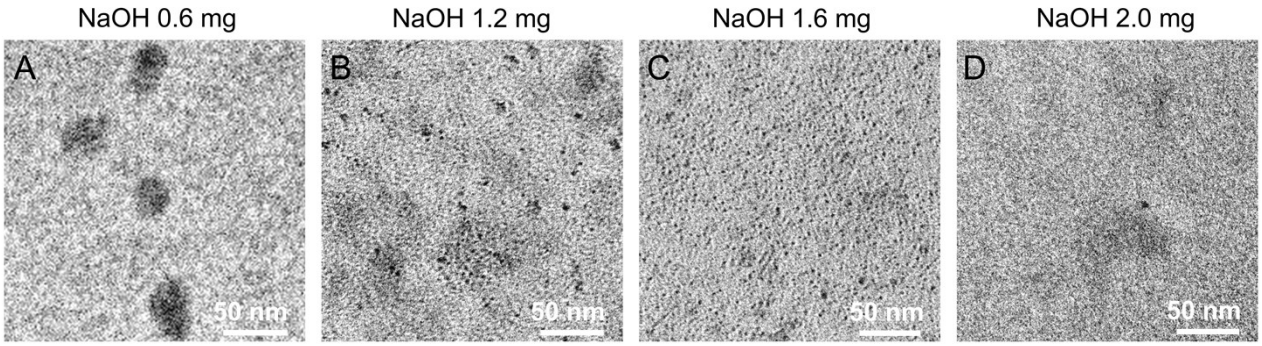

Figure S4. TEM images of PF NPs prepared with 30% His grafted polymer and different dosages of NaOH, (A) 0.6 mg (PF-30 NPs), (B) 1.2 mg (PF-5 NPs), (C) 1.6 mg (PF-3 NPs), and (D) 2.0 mg, respectively.

The histamine grafted amphiphilic polymer ($PSI_{OAM/His}$) with varying amounts of His was prepared by aminolysis of the lactam ring on the poly (succinimide) (PSI) polymer with His and oleylamine (OAm). The results of the characterization are displayed in Figure S2. The ^{1}H NMR spectra illustrate that the histamine grafted amphiphilic polymer exhibits a -CH_3 proton peak at δ 0.87 ppm, compared with the raw PSI (orange box), indicating the successful grafting of OAm. Proton peaks of imidazole at 7.56 and 6.83 ppm (blue box) confirm the presence of the grafted His block. These results provide substantial evidence for the successful synthesis of the amphiphilic polymer. Subsequently, perfluoro-15-crown-5-ether (PFCE) dispersed in dichloromethane was encapsulated by the amphiphilic polymer through forming an oil-in-water (O/W) emulsion under ultrasonication. Figure S3 demonstrates that the PF nanoparticles (NPs) prepared using 30% His grafted polymer exhibited homogeneous distribution. Moreover, with the gradual increase in the dosage of sodium hydroxide in the range of 0.6 – 1.6 mg, the size of PF NPs gradually decreases. Upon further addition of sodium hydroxide to 2.0 mg, the product transforms from regular spherical small nanoparticles into amorphous flocculates (Figure S4). Therefore, the His grafted ratio and the dosage of sodium hydroxide were optimized at 30% and 1.6 mg for the fabrication of PF NPs, respectively.

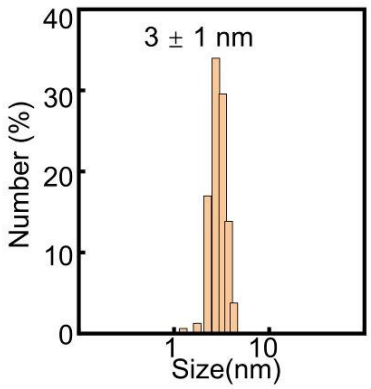

Figure S5. DLS size distribution of PF NPs prepared with 1.6 mg of NaOH and 30% His grafted polymer.

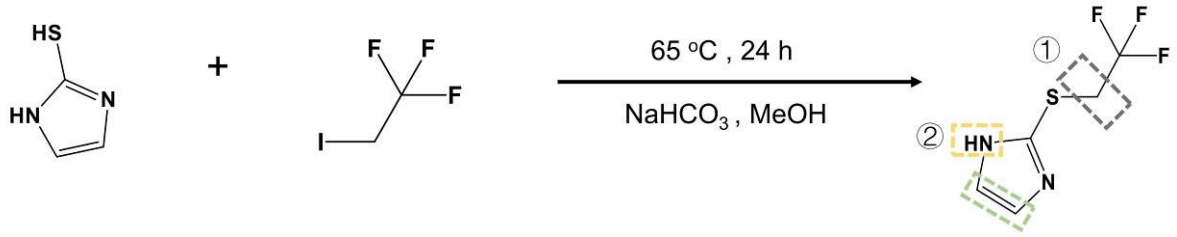

Figure S6. Synthetic routes of 2-((2,2,2-trifluoroethyl)thio)-1*H*-imidazole.

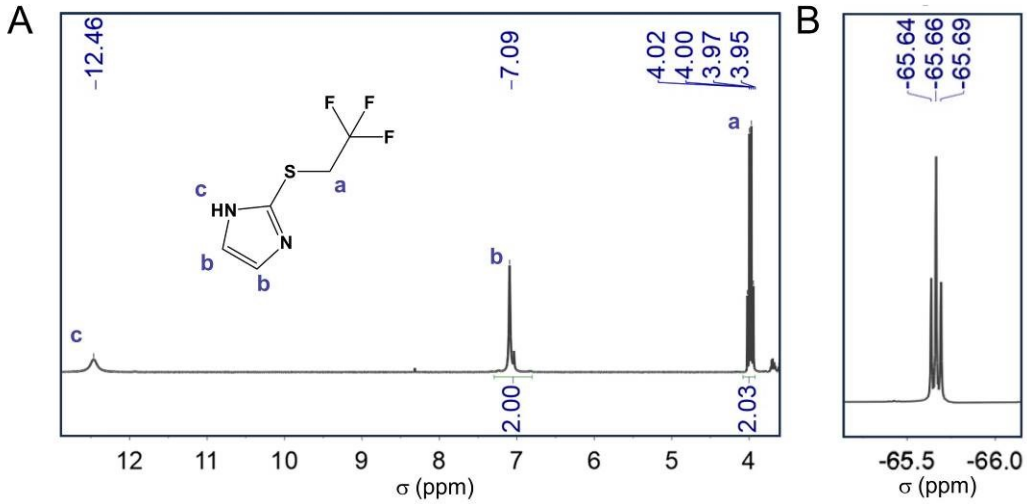

Figure S7. (A) ^{1}H NMR and (B) ^{19}F NMR spectra of 2-((2,2,2-trifluoroethyl)thio)-1*H*-imidazole. ^{1}H NMR(400 MHz, DMSO-*d*6), 7.09 (s, 2H), 3.98 (q, J = 10.3 Hz, 2H).

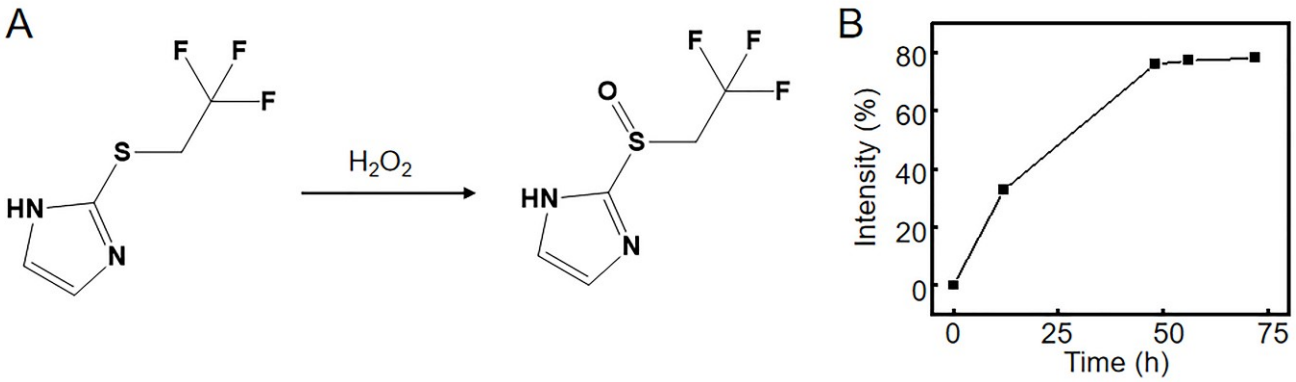

Figure S8. (A) Synthetic routes of 2-((2,2,2-trifluoroethyl)sulfinyl)-1*H*-imidazole. (B) Oxidation percentage at different oxidation times.

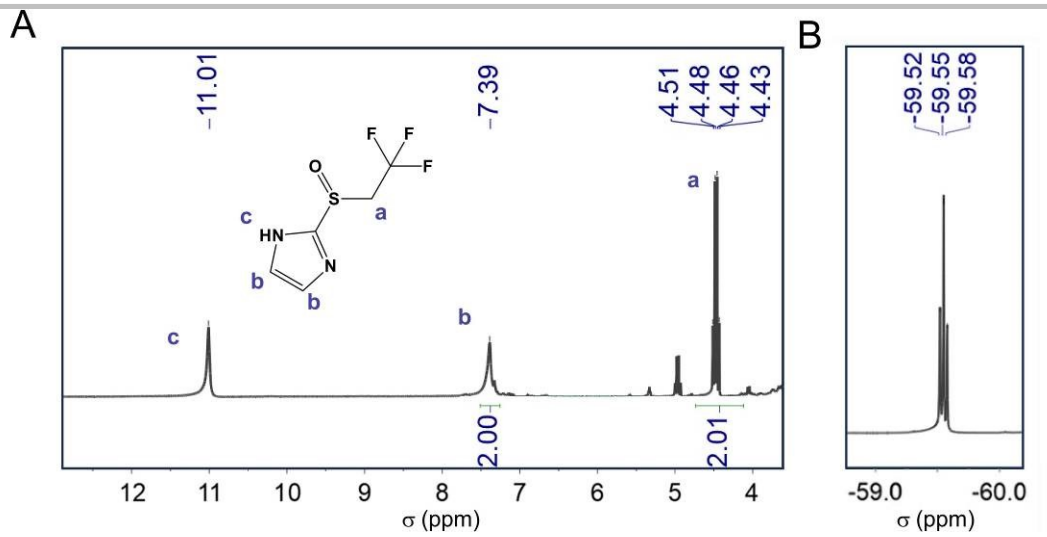

Figure S9. (A)^{1}H NMR and (B) ^{19}F NMR spectra of 2-((2,2,2-trifluoroethyl)sulfinyl)-1*H*-imidazole. ^{1}H NMR (400 MHz, DMSO-d6), 7.39 (s,2H), 4.47 (q, J-10.7 Hz, 2H).

The 2-((2,2,2-trifluoroethyl)thio)-1*H*-imidazole was oxidized with hydrogen peroxide, and the oxidation process was monitored by ^{19}F NMR on basis of the chemical shift of -CF_3. The peak position of -CF_3 connected to the thioether group before oxidation was around δ -66.87 ppm, which would shift to -60.98 ppm after oxidation. The conversion ratio from thioether to sulfoxide can be evaluated by calculating the integral areas of these two peaks (Figure S7B and S9B). As can be seen from Figure S8, the oxidation was finished at around 48 h with a conversion rate of 76%. As shown in Figure S9A, the ^{1}H NMR spectrum of 2-((2,2,2-trifluoroethyl)sulfinyl)-1*H*-imidazole (F-MIZ) showed a peak at 4.5 ppm, belonging to the methylene group attached to the sulfoxide group. These results indicate that the thioether group of F-MIZ was successfully oxidized to the sulfoxide by H_2O_2, which will greatly enhance the hydrophilicity and mobility of 2-((2,2,2-trifluoroethyl)sulfinyl)-1*H*-imidazole.

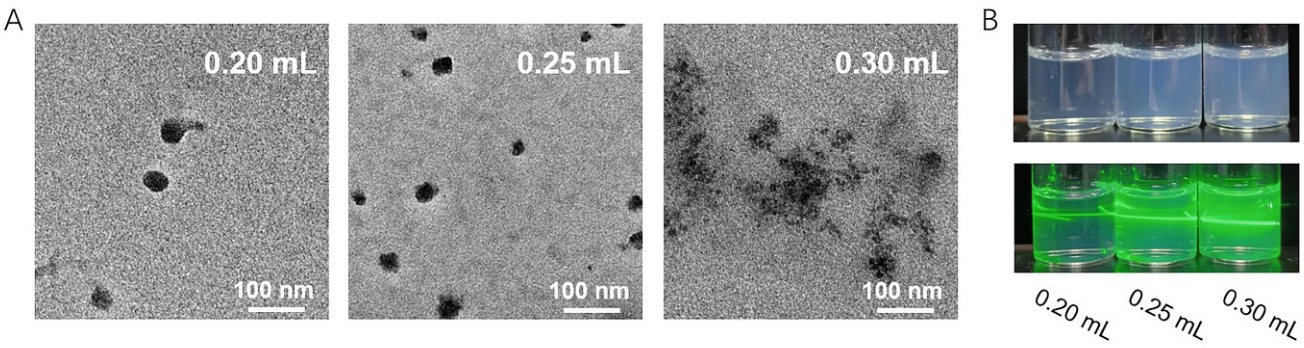

Figure S10. (A) TEM images of PFZF NPs (PF: PFCE nanodroplets; Z: Zn^{2+}; F: F-MIZ) prepared under different volumes (0.2, 0.25 and 0.3 mL) of $NH_3{\cdot}H_2O$ (0.25%). (B) Corresponding actual photographs of PFZF NPs colloidal solution.

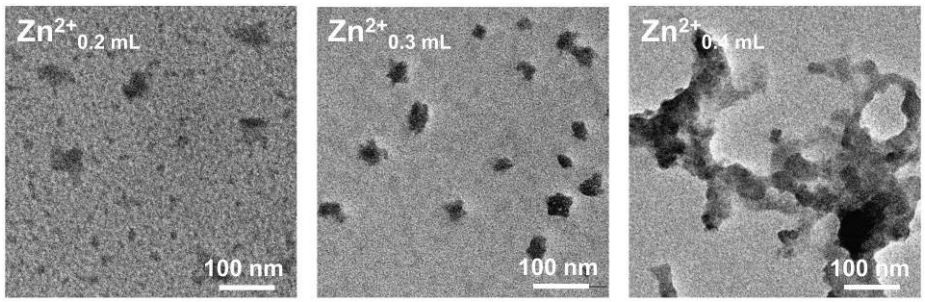

Figure S11. TEM images of PFZF NPs (PF: PFCE nanodroplets; Z: Zn^{2+}; F**:** F-MIZ) prepared with 0.25 mL of $NH_3{\cdot}H_2O$ (0.25%) and different amounts (0.2, 0.3 and 0.4 mL) of $Zn(NO_3)_2{\cdot}6H_2O$ (6.5 mg/mL), respectively.

The coordination bonds between F-MIZ and Zn^{2+} ions were found to be pH-dependent when preparing the trifluoromethyl-containing metal-organic assemblies. With an increase in the dosage of $NH_3 \cdot H_2O$, the quantity of nanoassemblies gradually increases. However, when the dosage of $NH_3 \cdot H_2O$ surpasses 0.25 mL, the product undergoes a transformation from regular spherical nanoparticles into amorphous agglomerates (Figure S10a). The photographs depict actual samples showing that, the Tyndall effect of the colloidal solution gradually intensifies as the dosage of $NH_3 \cdot H_2O$ increases during preparation (Figure S10b). The dosage of $NH_3 \cdot H_2O$ (0.25%) was optimized at 0.25 mL in this study. Furthermore, as shown in Figure S11, Zinc ions function as metallic nodes to connect histamine-grafted PF NPs and F-MIM, and the quantity of zinc ions added is critical in this process. An insufficient amount of zinc ions (0.2 mL) fails to assemble the histamine-grafted PF NPs and F-MIM. Conversely, when the amount of zinc ions is increased to 0.3 mL, it is adequate to assemble the histamine-grafted PF NPs and F-MIM, resulting in nanoparticles with a uniform distribution and a DLS size of approximately 54 ± 14nm (Figure S12). However, an excessive amount of zinc ions (0.4 mL) leads to the formation of larger amorphous assemblies. Therefore, the dosage of Zine ion (6.5 mg/mL) was optimized at 0.3 mL in this study.

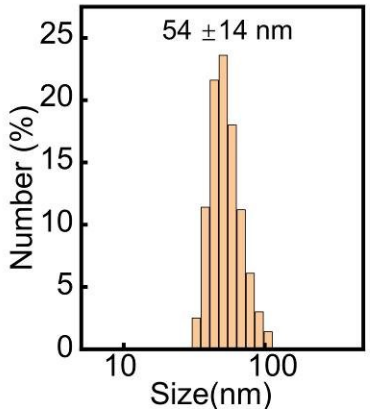

Figure S12. DLS size distribution of PFZF NPs prepared with 0.25 mL $NH_3 \cdot H_2O$ (0.25%) and 0.3 mL of $Zn(NO_3)_2 \cdot 6H_2O$ (6.5 mg/mL).

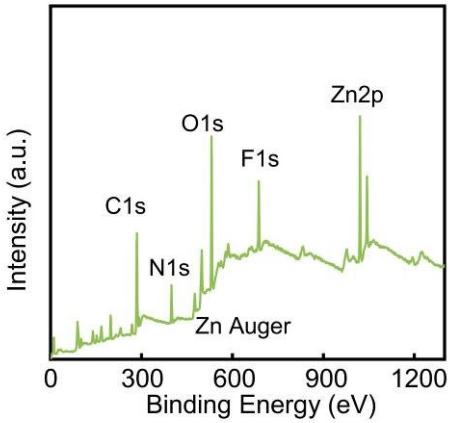

Figure S13. XPS of PFZF NPs.

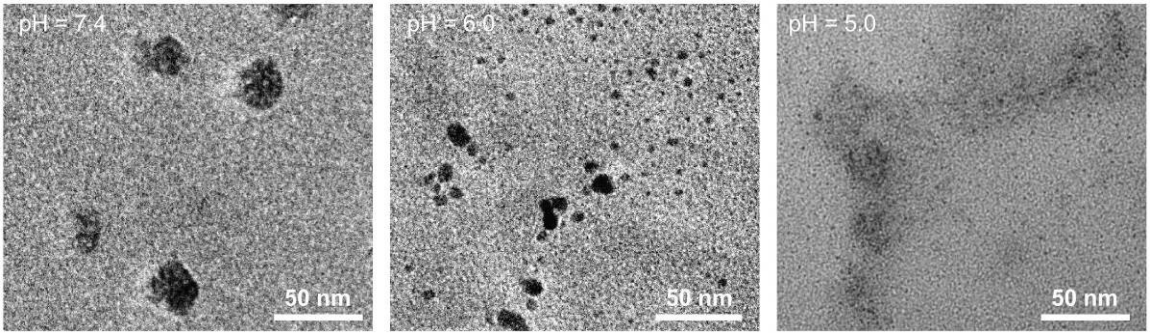

Figure S14. TEM images of PFZF NPs under different pH (7.4, 6.0 and 5.0), respectively.

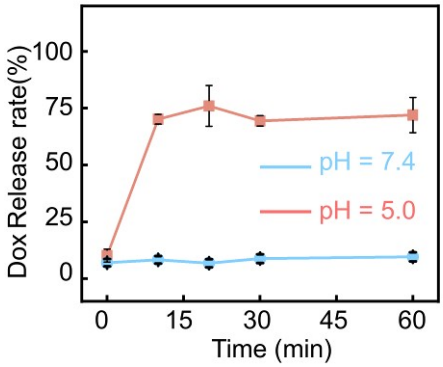

Figure S15. Cumulative release of Dox from PFZF-Dox NPs under different conditions along with time (n = 3 per condition). Error bars represent standard deviations.

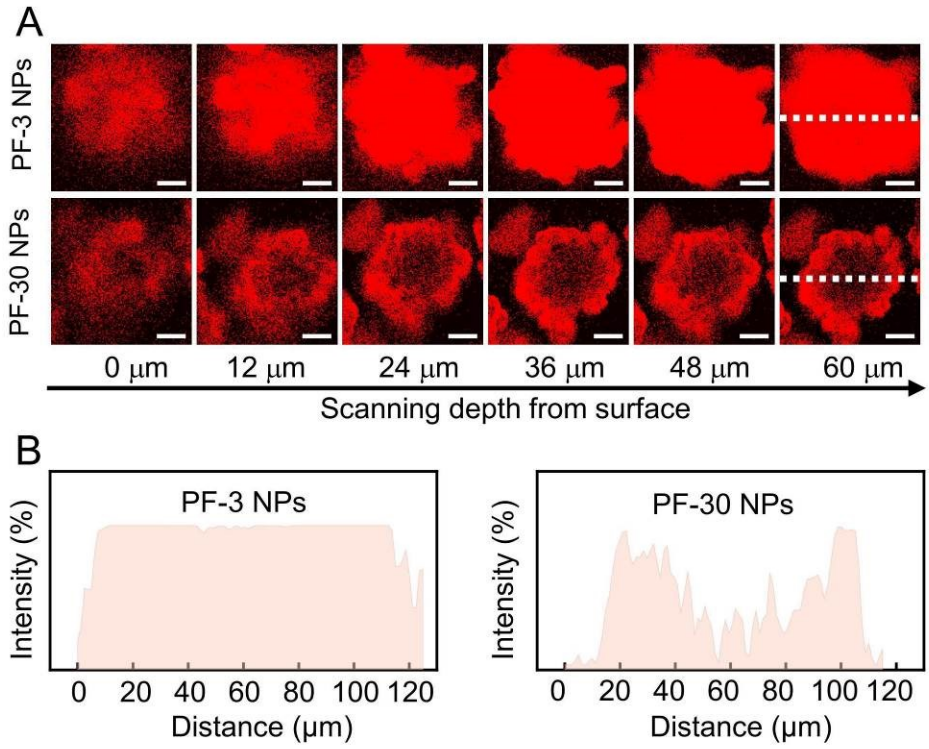

Figure S16. (A) Confocal fluorescence images of 4T1 3D tumor spheroids after incubation with PF3 and PF30 NPs (Scale bar = 25 μm). (B) Quantitative analysis of red fluorescence intensities in different groups for line scanning of 3D tumor spheroids at a given depth.

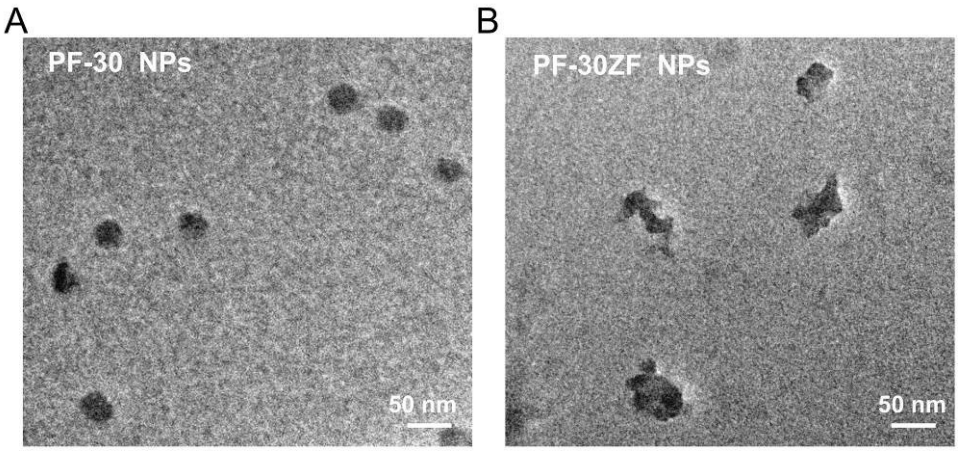

Figure S17. TEM images of PF-30 NPs and PF-30ZF NPs.

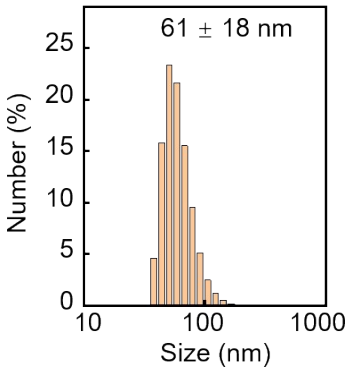

Figure S18. DLS size distribution of PF-30ZF NPs.

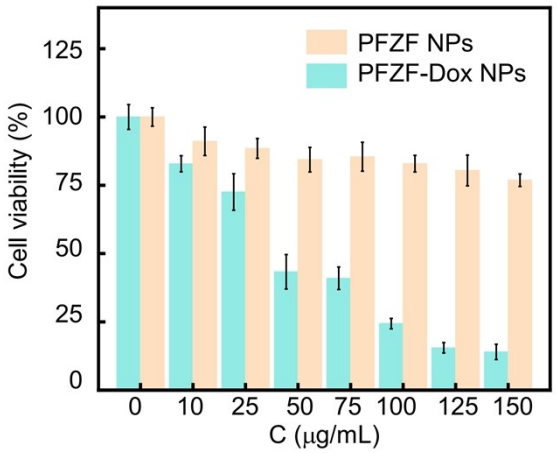

Figure S19. Cell viability of 4T1 cells exposed to different concentrations of PFZF NPs and PFZF-Dox NPs, respectively (n = 6).

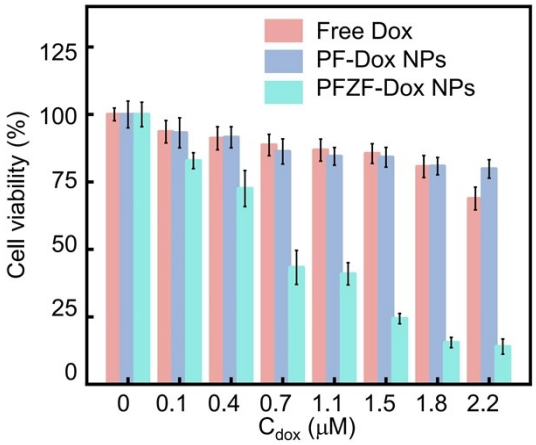

Figure S20. Cell viability of 4T1 cells exposed to different concentrations of free Dox, PF-Dox NPs, and PFZF-Dox NPs, respectively (n = 6).

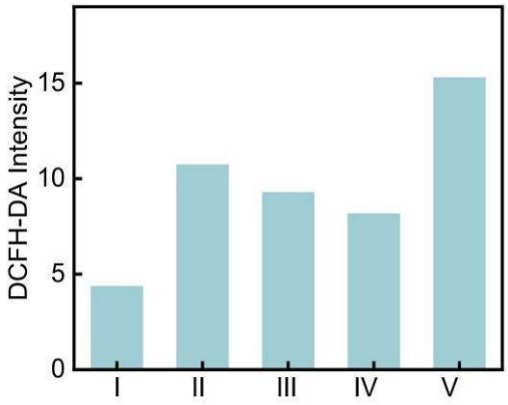

Figure S21. Quantitative data of fluorescence images of cells stained by DCFH-DA. I: PBS; II: PFZF NPs; III: Free Dox; IV: PF-Dox NPs; V: PFZF-Dox NPs.

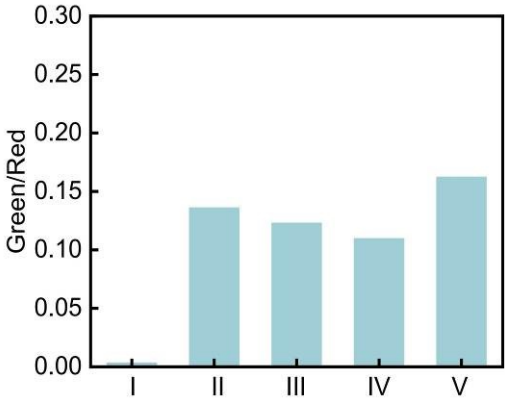

Figure S22. Quantitative data of fluorescence images of cells stained by JC-1. I: PBS; II: PFZF NPs; III: Free Dox; IV: PF-Dox NPs; V: PFZF-Dox NPs.

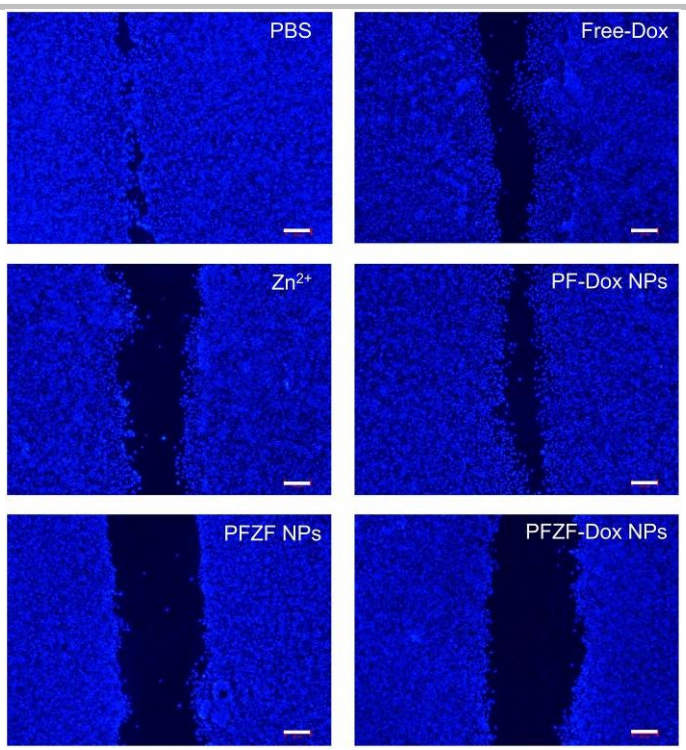

Figure S23. Cell migration assay of 4T1 cells after different formulations. The scale bar represents 60 μm.

As shown in Figure S23, compared with other groups, Zn^{2+}, PFZF, and PFZF-Dox groups have the best suppression effect on cell migration, which will prevent the metastasis of tumor cells, implying that inhibiting cell migration may be partially attributed to the growth hindrance of high concentration of Zinc.

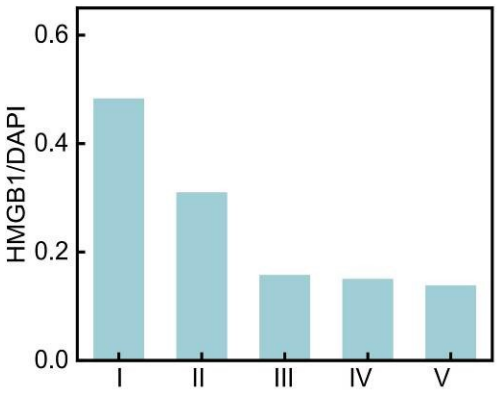

Figure S24. Quantitative data of fluorescence images of cells stained by HMGB1 fluorescent antibody and DAPI. I: PBS; II: PFZF NPs; III: Free Dox; IV: PF-Dox NPs; V: PFZF-Dox NPs.

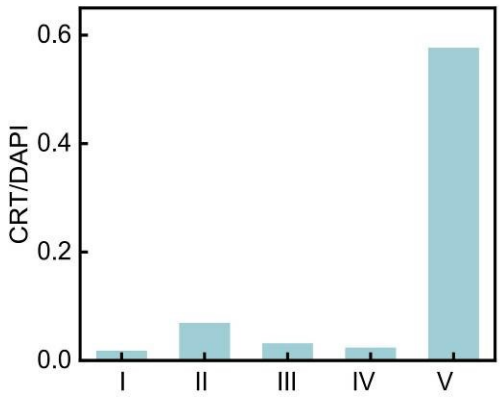

Figure S25. Quantitative data of fluorescence images of cells stained by CRT fluorescent antibody and DAPI. I: PBS; II: PFZF NPs; III: Free Dox; IV: PF-Dox NPs; V: PFZF-Dox NPs.

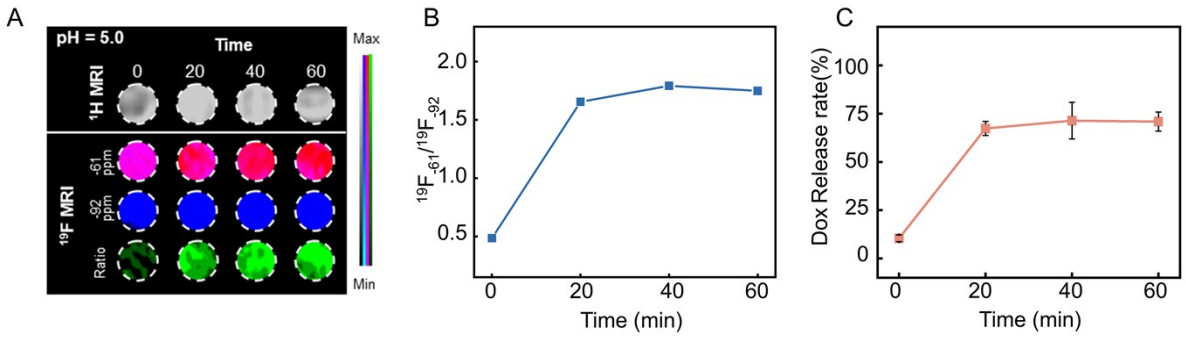

Figure S26. (A) ^{1}H MRI and ^{19}F MRI images of PFZF-Dox NPs suspension under pH 5.0 along with time. RF excitation pulse at −61 ppm (red channel) and -92 ppm (blue channel). (B) The plot of ^{19}F MRI intensity ratio ($^{19}F_{-61}/^{19}F_{-92}$) of PFZF-Dox NPs at different times. (C) The plot of Dox release percentage of PFZF-Dox NPs at different times (n = 3).

For proof-of-concept, PFZF-Dox NPs were dispersed in pH = 5.0 buffer solution to simulate the intracellular environment pH. This solution was kept at 37 °C for 60 min. The release of Dox at different time points was measured by UV-vis absorption spectroscopy, and ratiometric ^{19}F MRI signals were also quantified at each time point. As shown in Figure S26, the ratiometric ^{19}F MRI signals change corresponded with the Dox release rate across the different time points of the release process, which reached the plateau at 20 min.

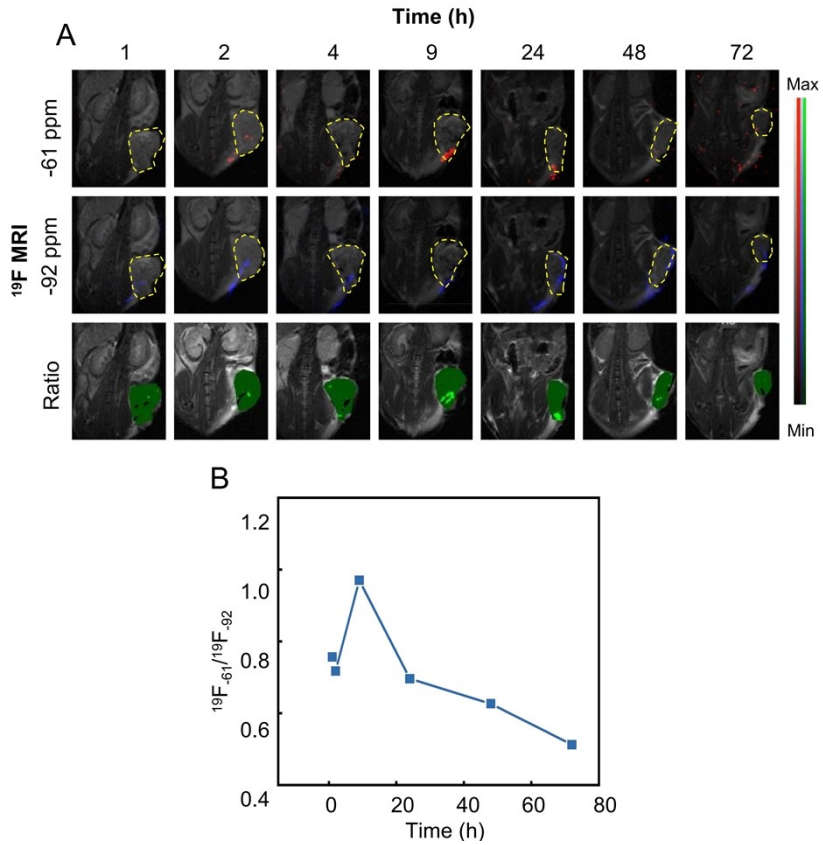

Figure S27. (A) ^{19}F MRI of 4T1 tumor-bearing mice at different time peritumoral injections. (B) Quantitative data of $^{19}F_{-61}/^{19}F_{-92}$ obtained from Figure S27A.

We tested the ^{19}F MRI at different time points after peritumoral injections of PFZF-Dox NPs (Fig. S27). From the ^{19}F MRI signal at -92 ppm (blue channel), it was identified that most of the PFZF-Dox NPs were predominantly localized around the tumor within the first 1 h and permeated to the tumor gradually. Then, the intensity of the ^{19}F MRI signals at -92 ppm (blue channel) from the tumor reached a saturated level (24 h), followed by a gradual decline due to clearance from the mouse. In contrast, the intensity of the ^{19}F MRI signal at -61 ppm (red channel) exhibited a rapid increase at 9 h, subsequently decreasing gradually. The ratiometric ^{19}F MRI signal ($^{19}F_{-61}/^{19}F_{-92}$) reached peak values at the 9 h. Subsequent changes in the signal proved difficult to quantify due to the impact of metabolic processes, thus complicating the analysis. Moreover, both red and blue channel signals disappeared by 96 hours post-injection. Given these observations, a four-day injection interval was chosen, supporting the chosen dosing schedule.

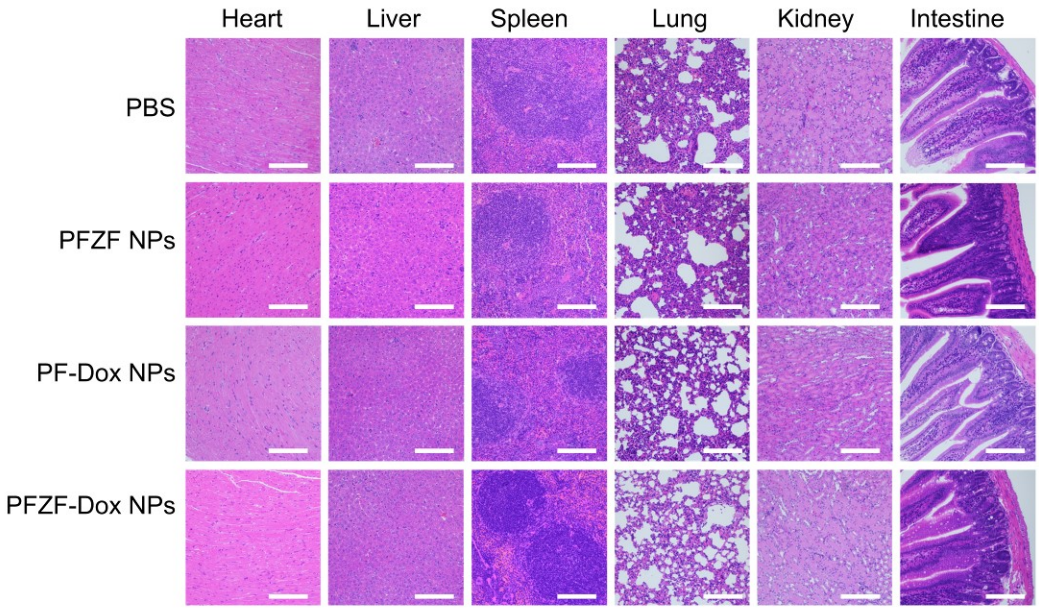

Figure S28. H&E stained images of main organs from mice after different treatments (Scale bar = 100 μm).

Table S1. A table describing the composition of specific materials.

Name	Composition	Size/nm
PF-3 NPs	PFCE, PSIOAm/His	3.0 ± 0.6
PF-5 NPs	PFCE, PSIOAm/His	5 ± 1
PF-30 NPs	PFCE, PSIOAm/His	32 ± 6
PF-Dox NPs (PF-3 NPs encapsulating Dox)	PFCE, Dox, PSIOAm/His	3.0 ± 0.7
PFZF NPs (PF-3 NPs coating with F-MIZ-Zn^{2+} complex)	PF-3 NPs, Zn^{2+}, F-MIZ	54 ± 14
PF-30ZF NPs	PF-30 NPs, Zn^{2+}, F-MIZ	61 ± 18
PFZF-Dox NPs (PFZF NPs encapsulating Dox)	PF-Dox NPs, Zn^{2+}, F-MIZ	47 ± 11